GEOPHYSICS, VOL. 68, NO. 2 (MARCH-APRIL 2003); P. 535–543, 11 FIGS., 3 TABLES.
10.1190/1.1567222

A least-squares derivatives analysis of gravity anomalies due to faulted thin slabs

El-Sayed M. Abdelrahman*, Hesham M. El-Araby*, Tarek M. El-Araby*, and Eid Ragab Abo-Ezz*

ABSTRACT

This paper presents two different least-squares approaches for determining the depth and amplitude coefficient (related to the density contrast and the thickness) of a buried faulted thin slab from numerical first-, second-, third-, and fourth-horizontal derivative anomalies obtained from 2D gravity data using filters of successive graticule spacings. The problem of depth determination has been transformed into the problem of finding a solution to a nonlinear equation of the form $f(z) = 0$. Knowing the depth and applying the least-squares method, the amplitude coefficient is determined using a simple linear equation. In this way, the depth and amplitude coefficient are determined individually from all observed gravity data. The depths and the amplitude coefficients obtained from the first-, second-, third-, and fourth- derivative anomaly values can be used to determine simultaneously the actual depth and amplitude coefficient of the buried fault structure and the optimum order of the regional gravity field along the profile. The method can be applied not only to residuals but also to the Bouguer anomaly profile consisting of the combined effect of a residual component due to a purely local fault structure (shallow or deep) and a regional component represented by a polynomial of any order. The method is applied to theoretical data with and without random errors and is tested on a field example from Egypt.

INTRODUCTION

In gravity interpretation, faults are usually approximated by one or more semiinfinite beds terminated by vertical or dipping faults (Hedstrom, 1938; Hubbert, 1948; Geldert et al., 1966; Grant and West, 1970). However, in many exploration problems, it is valid to assume a faulted structure that can be represented by a faulted thin slab. The model may not be entirely geologically realistic, but it is frequently used in gravity interpretation to find the depth and thickness of a class of faulted structures. In most cases, the density contrast is assumed, and the depth and thickness may be obtained by graphical methods (Nettleton, 1976) and least-squares approaches (Gupta, 1983; Lines and Treitel, 1984). However, the accuracy of the results obtained by these methods depends on the accuracy with which the residual anomaly can be separated from the observed gravity anomaly.

On the other hand, Abdelrahman et al. (1989) show that correlation factors between successive least-squares residual gravity anomalies from a buried faulted thin slab can be used to extract depth and regional gravity field information. The drawback with this approach is that it can not be applied to interpret all gravity data points acquired on a large area over the buried structure (i.e., from the long segment of the gravity profile around the origin). In this case, the correlation factors would be independent of the depth and would be only a function of the orders of the regional polynomial used (Abdelrahman et al., 1985). Moreover, the correlation factors method (Abdelrahman et al., 1989) is considered as a semiautomatic technique for determining the model parameters of faulted structures from gravity data.

Here, we present a full automatic method that uses two different least-squares approaches to determine the depth and amplitude coefficient of a buried faulted thin slab, successively from numerical first-, second-, third-, and fourth-derivative anomalies obtained from observed 2D gravity data using filters of successive graticule spacings. The model parameters obtained from the different numerical derivative anomaly values can be used to determine simultaneously the actual model parameters of the buried fault and the optimum order of the regional gravity field along the profile. The validity of the method is tested on theoretical examples with and without random errors and on a field example from Egypt.

Manuscript received by the Editor August 10, 2001; revised manuscript received August 24, 2002.
*Cairo University, Geophysics Department, Faculty of Science, Giza, Egypt. E-mail: sayed5005@yahoo.com.

THE LEAST-SQUARES DERIVATIVES ANALYSIS METHOD

Following Nettleton (1976), the expression for the gravity anomaly from a faulted thin slab is

$$g(x_i, z) = K\left\{\frac{1}{2} + \frac{1}{\pi}\tan^{-1}\left(\frac{x_i}{z}\right)\right\}, \quad i = 1, 2, 3 \ldots N \tag{1}$$

where $K = 2\pi G\sigma t$ and $z/2 \geq t$. In equation (1), z is depth, x is the horizontal position coordinate, σ is the density contrast, G is the universal gravitational constant, and t is the thickness of the slab. (Nomenclature is summarized in Table 1.) The fault model is equivalent to a horizontal sheet, which is cut of at a vertical plane below point 0 (Figure 1). For this case, the material is considered as being condensed onto a thin sheet, or lamina, of mass σt per unit area and at a depth z, coresponding to the center of the original slab (Figure 1).

Consider observation points, $x_i - M, \ldots, x_i - 2s, x_i - s, x_i, x_i + s, x_i + 2s, \ldots, x_i + M$ along the anomaly profile where $s = 1, 2, 3, \ldots, M$ spacing units and is called the graticule spacing or numeric sampling interval. The first horizontal gradient is

$$g_x(x_i, z, s) = \frac{K}{2\pi s}\left\{\tan^{-1}\left(\frac{x_i + s}{z}\right) - \tan^{-1}\left(\frac{x_i - s}{z}\right)\right\}. \tag{2}$$

Equation (2) gives the following value at $x_i = 0$:

$$g_x(0) = \frac{K}{\pi s}\left\{\tan^{-1}\left(\frac{s}{z}\right)\right\}, \tag{3}$$

Table 1. Nomenclature.

x	Distance along traverse from local origin.
k	Amplitude coefficient related to depth and thickness of the faulted thin slab.
G	Universal gravitational constant.
σ	Density contrast across a faulted thin slab.
z	Depth to the center of the faulted thin slab.
t	Thickness of the faulted thin slab.
s	Graticule spacing.
N	Number of data points along traverse.
$g_x(x, z, s)$	First horizontal derivative of gravity in the traverse direction.
$g_{xx}(x, z, s)$	Second horizontal derivative of gravity in the traverse direction.
$g_{xxx}(x, z, s)$	Third horizontal derivative of gravity in the traverse direction.
$g_{xxxx}(x, z, s)$	Fourth horizontal derivative of gravity in the traverse direction.
$g_x(0)$	Value of $g_x(x, z, s)$ at $x = 0$.
$g_{xx}(s)$	Value of $g_{xx}(x, z, s)$ at $x = s$.
$g_{xxx}(0)$	Value of $g_{xxx}(x, z, s)$ at $x = 0$.
$g_{xxxx}(s)$	Value of $g_{xxxx}(x, z, s)$ at $x = s$.

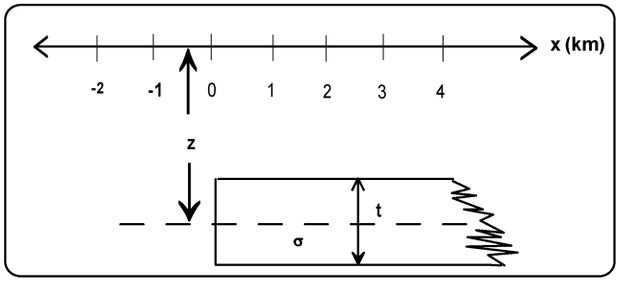

FIG. 1. Geometry of the faulted thin slab model.

Using equation (3), equation (2) can be written as

$$g_x(x_i, z, s) = g_x(0)W_x(x_i, z, s), \tag{4}$$

where

$$W_x(x_i, z, s) = \frac{\tan^{-1}\left(\frac{x_i + s}{z}\right) - \tan^{-1}\left(\frac{x_i - s}{z}\right)}{2\tan^{-1}\left(\frac{s}{z}\right)}.$$

The unknown depth (z) in equation (4) can be obtained by minimizing

$$\varphi(z) = \sum_{i=1}^{N}[L(x_i) - g_x(0)W_x(x_i, z, s)]^2, \tag{5}$$

where $L(x_i)$ denotes the numerical horizontal gradient.

Setting the derivative of $\phi(z)$ to zero with respect to z leads to the following equation:

$$f(z) = \sum_{i=1}^{N}[L(x_i) - g_x(0)W_x(x_i, z, s)]W_x^*(x_i, z, s) = 0, \tag{6}$$

where

$$W_x^*(x_i, z, s) = \frac{dW_x(x_i, z, s)}{dz}.$$

Equation (6) can be solved using the standard methods for solving nonlinear equations. Here, it is solved by a simple iteration method (Press et al., 1986).

Substituting the computed depth (z_c) as a fixed parameter in equation (2), we obtain

$$g_x(x_i, s) = \frac{K}{2\pi s}\left\{\tan^{-1}\left(\frac{x_i + s}{z_c}\right) - \tan^{-1}\left(\frac{x_i - s}{z_c}\right)\right\}. \tag{7}$$

Again, applying the least-squares method, the unknown K in equation (7) can be obtained from the following equation:

$$K = \frac{2\pi s\sum_{i=1}^{N}\left[L(x_i)\left\{\tan^{-1}\left(\frac{x_i + s}{z_c}\right) - \tan^{-1}\left(\frac{x_i - s}{z_c}\right)\right\}\right]}{\sum_{i=1}^{N}\left[\tan^{-1}\left(\frac{x_i + s}{z_c}\right) - \tan^{-1}\left(\frac{x_i - s}{z_c}\right)\right]^2}. \tag{8}$$

Knowing K, the thickness of the faulted slab can be determined from the relationship given in equation (1).

The second horizontal gradient is

$$g_{xx}(x_i, z, s) = \frac{K}{4\pi s^2}\left\{\tan^{-1}\left(\frac{x_i + 2s}{z}\right) - 2\tan^{-1}\left(\frac{x_i}{z}\right) + \tan^{-1}\left(\frac{x_i - 2s}{z}\right)\right\}. \tag{9}$$

Again, equation (9) can be written as

$$g_{xx}(x_i, z, s) = g_{xx}(s)W_{xx}(x_i, z, s), \tag{10}$$

where

$$W_{xx}(x_i, z, s) = \frac{\left\{\tan^{-1}\left(\frac{x_i + 2s}{z}\right) - 2\tan^{-1}\left(\frac{x}{z}\right) + \tan^{-1}\left(\frac{x_i - 2s}{z}\right)\right\}}{\left\{\tan^{-1}\left(\frac{3s}{z}\right) - 3\tan^{-1}\left(\frac{s}{z}\right)\right\}},$$

and where $g_{xx}(s)$ is the second derivative anomaly value at $x_i = s$.

Following the same approach used to derive equation (6), the depth can be obtained from the numerical second horizontal gradient anomaly values ($H(x_i)$) by minimizing

$$\lambda(z) = \sum_{i=1}^{N} [H(x_i) - g_{xx}(s) W_{xx}(x_i, z, s)]^2, \tag{11}$$

which yields the following nonlinear equation in z:

$$f(z) = \sum_{i=1}^{N} [H(x_i) - g_{xx}(s) W_{xx}(x_i, z, s)]\, W^*_{xx}(x_i, z, s) = 0, \tag{12}$$

where

$$W^*_{xx}(x, z, s) = \frac{dW_{xx}(x, z, s)}{dz}.$$

Substituting the computed depth (z_c) in equation (9) and applying the least-squares method, the amplitude coefficient is obtained from the following equation:

$$K = \frac{4\pi s^2 \sum_{i=1}^{N} H(x_i) \left[\tan^{-1}\left(\frac{x_i + 2s}{z_c}\right) - 2\tan^{-1}\left(\frac{x_i}{z_c}\right) + \tan^{-1}\left(\frac{x_i - s}{z_c}\right)\right]}{\sum_{i=1}^{N} \left[\tan^{-1}\left(\frac{x_i + 2s}{z_c}\right) - 2\tan^{-1}\left(\frac{x_i}{z_c}\right) + \tan^{-1}\left(\frac{x_i - s}{z_c}\right)\right]^2}, \tag{13}$$

The third horizontal gradient is

$$g_{xxx}(x_i, z, s) = \frac{K}{8\pi s^3}\left\{ \tan^{-1}\left(\frac{x_i + 3s}{z}\right) - 3\tan^{-1} \times \left(\frac{x_i + s}{z}\right) + 3\tan^{-1}\left(\frac{x_i - s}{z}\right) - \tan^{-1}\left(\frac{x_i - 3s}{z}\right)\right\}, \tag{14}$$

which yields

$$f(z) = \sum_{i=1}^{N} [P(x_i) - g_{xxx}(0) W_{xxx}(x_i, z, s)] W^*_{xxx}(x_i, z, s) = 0, \tag{15}$$

and

$$K = \frac{8\pi s^3 \sum_{i=1}^{N} L(x_i) \left[\tan^{-1}\left(\frac{x_i + 3s}{z_c}\right) - 3\tan^{-1}\left(\frac{x_i + s}{z_c}\right) + 3\tan^{-1}\left(\frac{x_i - s}{z_c}\right) - \tan^{-1}\left(\frac{x_i - 3s}{z_c}\right)\right]}{\sum_{i=1}^{N} \left[\tan^{-1}\left(\frac{x_i + 3s}{z_c}\right) - 3\tan^{-1}\left(\frac{x_i + s}{z_c}\right) + 3\tan^{-1}\left(\frac{x_i - s}{z_c}\right) - \tan^{-1}\left(\frac{x_i - 3s}{z_c}\right)\right]^2}, \tag{16}$$

where

$$W_{xxx}(x_i, z, s) = \frac{\tan^{-1}\left(\frac{x_i + 3s}{z}\right) - 3\tan^{-1}\left(\frac{x_i + s}{z}\right) + 3\tan^{-1}\left(\frac{x_i - s}{z}\right) - \tan^{-1}\left(\frac{x_i - 3s}{z}\right)}{2\tan^{-1}\left(\frac{3s}{z}\right) - 6\tan^{-1}\left(\frac{s}{z}\right)},$$

and

$$W^*_{xxx}(x, z, s) = \frac{dW_{xxx}(x, z, s)}{dz},$$

and where $P(x_i)$ denotes the numerical third horizontal gradient anomaly values.

Finally, the fourth horizontal gradient is

$$g_{xxxx}(x_i, z, s) = \frac{K}{16\pi s^4}\left\{ \tan^{-1}\left(\frac{x_i + 4s}{z}\right) - 4\tan^{-1}\left(\frac{x_i + 2s}{z}\right) + 6\tan^{-1}\left(\frac{x_i}{z}\right) - 4\tan^{-1}\left(\frac{x_i - 2s}{z}\right) + \tan^{-1}\left(\frac{x_i - 4s}{z}\right)\right\}, \tag{17}$$

which yields

$$f(z) = \sum_{i=1}^{N} [R(x_i) - g_{xxxx}(s) W_{xxxx}(x_i, z, s)] \times W^*_{xxxx}(x_i, z, s) = 0, \tag{18}$$

and

$$K = \frac{16\pi s^4 \sum_{i=1}^{N} R(x_i)\left[\tan^{-1}\left(\frac{x_i+4s}{z_c}\right) - 4\tan^{-1}\left(\frac{x_i+2s}{z_c}\right) + 6\tan^{-1}\left(\frac{x_i}{z_c}\right) - 4\tan^{-1}\left(\frac{x_i-2s}{z_c}\right) + \tan^{-1}\left(\frac{x_i-4s}{z_c}\right)\right]}{\sum_{i=1}^{N}\left[\tan^{-1}\left(\frac{x_i+4s}{z_c}\right) - 4\tan^{-1}\left(\frac{x_i+2s}{z_c}\right) + 6\tan^{-1}\left(\frac{x_i}{z_c}\right) - 4\tan^{-1}\left(\frac{x_i-2s}{z_c}\right) + \tan^{-1}\left(\frac{x_i-4s}{z_c}\right)\right]^2}, \tag{19}$$

where

$$W_{xxxx}(x_i z, s) = \frac{\left\{\tan^{-1}\left(\frac{x_i+4s}{z}\right) - 4\tan^{-1}\left(\frac{x_i+2s}{z}\right) + 6\tan^{-1}\left(\frac{x_i}{z}\right) - 4\tan^{-1}\left(\frac{x_i-2s}{z}\right) + \tan^{-1}\left(\frac{x_i-4s}{z}\right)\right\}}{\left\{\tan^{-1}\left(\frac{5s}{z}\right) - 5\tan^{-1}\left(\frac{3s}{z}\right) + 10\tan^{-1}\left(\frac{s}{z}\right)\right\}}$$

and

$$W^*_{xxxx}(x, z, s) = \frac{dW_{xxxx}(x, z, s)}{dz},$$

and where $R(x_i)$ denotes the fourth horizontal gradient anomaly values.

Theoretically, any graticule spacing s is enough to determine the depth (z) and the amplitude coefficient K from the first-, second-, third, and fourth-derivative anomalies. In practice, more than one value of s is desirable because of the presence of noise and regional components in the data.

SYNTHETIC EXAMPLES

Synthetic examples of a faulted thin slab buried at different depths (profile length = 50 km, sampling interval = 1 km, and $k = 50$ mGal) were interpreted using the two least-squares methods [equations (6) and (8), (12) and (13), (15) and (16), and (18) and (19)] to determine, respectively, depths and amplitude coefficients from numerical derivative anomaly values. In all cases examined, the exact values of z and k were obtained. However, in studying the error response of the least-squares methods, synthetic examples contaminated with 5% random errors were considered. Following the interpretation method, values of the model parameters (z, k) were computed and the percentage of error in model parameters were plotted against the model depth for comparison (Figures 2 and 3).

We verified numerically that the depth and amplitude coefficient obtained are within 4.5%. It was also verified that the percentage of error in depth and amplitude coefficient does not depend on the derivative method itself (first, second, third, or fourth). It was also shown that the method works well when the structure is shallow or deep (Figures 2 and 3).

OPTIMUM-ORDER REGIONAL DETERMINATION

Geologic interpretation of geophysical data invariably involves the isolation of the geophysical anomaly in the presence of unwanted (or regional) data. Interpretation usually requires the subtraction of an estimated regional effect from the observed profile. However, this may result in serious distortions in magnitude and extension of local gravity anomalies. Other approaches to this problem are, for example, the radial weight methods (Griffin, 1949), the fast Fourier transform methods (Mesko, 1984), the rational approximation techniques (Agarwal and Lal, 1971), and application of recursion filters (Bhattacharyya, 1976). In addition to the above techniques, polynomial fitting by the least-squares method is an effective technique for separation of gravity anomalies into residual and regional components (Xia et al., 1996). Abdelrahman et al. (1989) presented a procedure to select the optimum polynomial order based on the correlation factors between residuals of successive orders. Zeng (1989) showed that the optimum order of the regional could be estimated from the point of discontinuity of the gradient on a graph of variance against the polynomial degree. That graph is obtained by fitting polynomials of different orders to an upward continuation of the observed anomaly at a proper height. In the present work, a simple procedure to determine the optimum order of the regional gravity field along the anomaly profile and to obtain the actual depth and amplitude coefficient of the buried structure is formulated as follows.

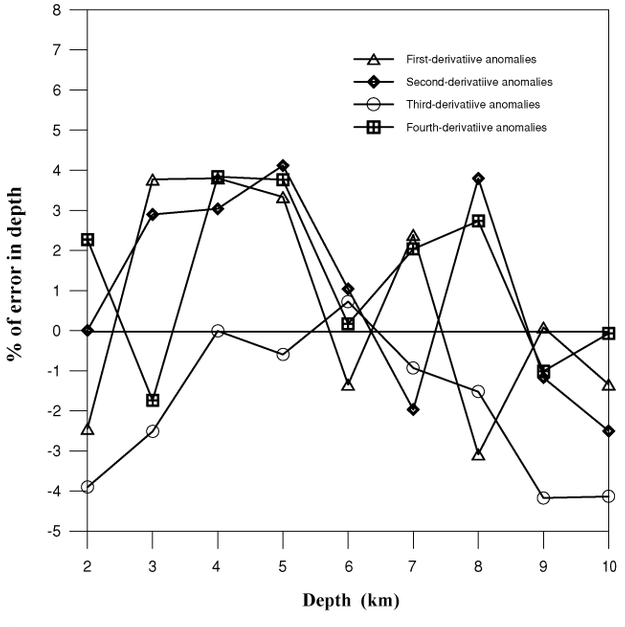

FIG. 2. Error response in depth parameter estimates. Abscissa: model depth. Ordinate: percent error in depth parameter.

The depths and amplitude coefficients of faulted thin slab computed from the different derivative anomalies can be used to determine the optimum order of the regional field and to estimate the depth and amplitude coefficient of the buried fault. The following 3 cases are given for illustration.

Case 1.—If the depths and amplitude coefficients, (z_1 and k_1) and (z_2 and k_2) of the buried faulted slab computed from the first-derivative anomalies and second-derivative anomalies are equal, then the regional is represented by a zero-order polynomial, and the true depth and amplitude coefficients are (z_1 and k_1). This is true because both first- and second-derivative operations remove the zero-order regional gravity field from the data.

Case 2.—If (z_1 and k_1) $\neq$ (z_2 and k_2) and (z_2 and k_2) = (z_3 and k_3), where (z_3 and k_3) are computed from the third-derivative anomalies, then the optimum order of the regional can be represented by a first-order polynomial and the true depth and amplitude coefficients are (z_2 and k_2). In this case, the first-derivative anomalies are distorted by the unremoved first-order regional.

Case 3.—If the regional is represented by a second-order polynomial, then (z_1 and k_1) $\neq$ (z_2 and k_2) and (z_2 and k_2) $\neq$ (z_3 and k_3), but (z_3 and k_3) = (z_4 and k_4), where (z_4 and k_4) are computed from the fourth-derivative anomalies, and so on.

THEORETICAL EXAMPLES

We compute a theoretical gravity field consisting of the combined effect of a fixed residual component and a regional component of three orders at 51 points with spacing of 1 depth unit. The residual component is represented by the gravity effect of a faulted thin slab ($z = 3$ km, and $K = 50$ mGal). The regional component $Z_p(x_i)$ of order p is represented successively by each of the following polynomials (orders 0 , 1, and 2):

$$Z_0(x_i) = 15, \qquad \text{(zero-order regional)} \tag{20}$$

$$Z_1(x_i) = x_i - 20, \qquad \text{(first-order regional)} \tag{21}$$

and

$$Z_2(x_i) = 0.023\,(x_i - 25)^2 + 0.2\,(x_i - 25) + 10. \qquad \text{(second-order regional)} \tag{22}$$

Each of these three regional components is added to the residual field to obtain three profiles Δg_1, Δg_2, and Δg_3, representing theoretical composite gravity fields of orders 0, 1, and 2, respectively (Figures 4–6). Each profile of the composite field is subjected to separation techniques using the numerical derivative methods.

The numerical values of the derivative anomaly can be computed from the observed data from the following equations:

$$g_x(x_i) = \frac{g(x_i + s) - g(x_i - s)}{2s} \tag{23}$$

for the first-derivative anomalies;

$$g_{xx}(x_i) = \frac{g(x_i + 2s) - 2g(x_i) + g(x_i - 2s)}{4s^2} \tag{24}$$

for the second-derivative anomalies;

$$g_{xxx}(x_i) = \frac{g(x_i + 3s) - 3g(x_i + s) + g(x_i - s) - g(x_i - 3s)}{8s^3} \tag{25}$$

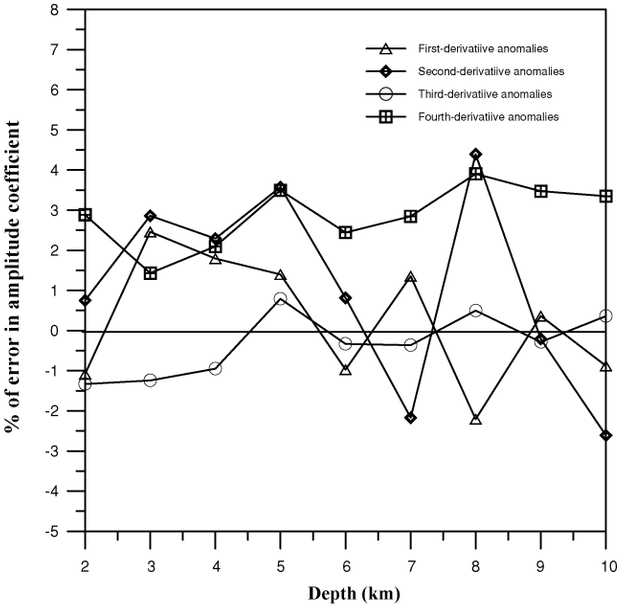

FIG. 3. Error response in amplitude coefficient parameter estimates. Abscissa: model depth. Ordinate: percent error in amplitude coefficient parameter.

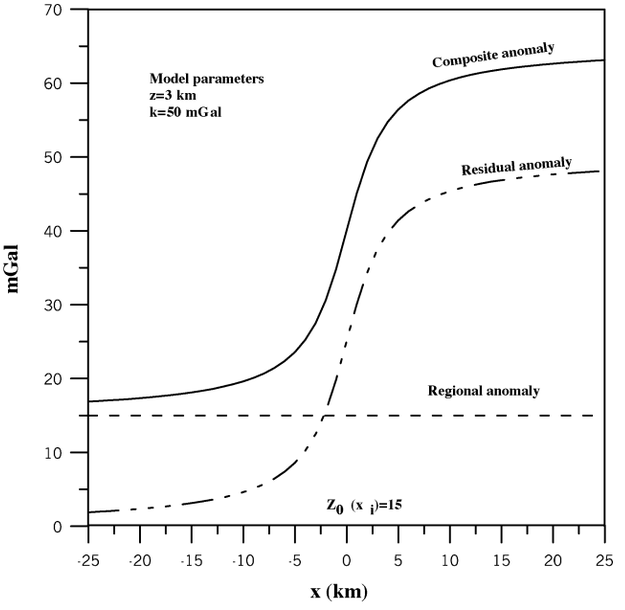

FIG. 4. Composite gravity anomaly Δg_1 of a buried faulted thin slab and a zero-order regional.

for the third-derivative anomalies; and

$$g_{xxxx}(x_i) = \frac{g(x_i+4s)-4g(x_i+2s)+6g(x_i)-4g(x_i-2s)+g(x_i-4s)}{16s^4} \quad (26)$$

for the fourth-derivative anomalies.

Three successive first-, second-, third- and fourth-derivative graticule spacings ($s = 2, 3$, and 4 km) were applied to each set of input data. Equations (6) and (8), (12) and (13), (15) and (16), and (18) and (19) are then applied to obtain the depths and the amplitude coefficients (z_1, k_1), (z_2, k_2), (z_3, k_3), and (z_4, k_4) from the numerical first-, second-, third-, and fourth-derivative anomalies, respectively. The numerical results of this study are shown in Table 2 for the zero-, first-, and second-order theoretical composite gravity fields. In Table 2, the average depth and amplitude coefficient estimates derived from the different derivatives are computed with their standard deviations to quantify the results.

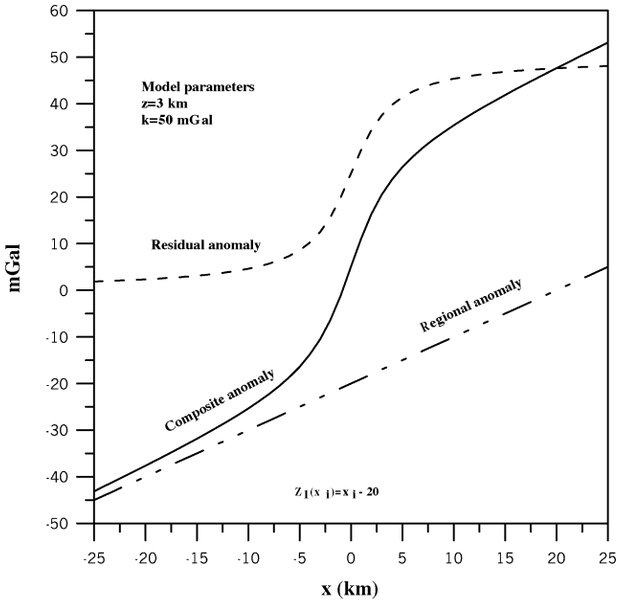

FIG. 5. Composite gravity anomaly Δg_2 of a buried faulted thin slab and a first-order regional.

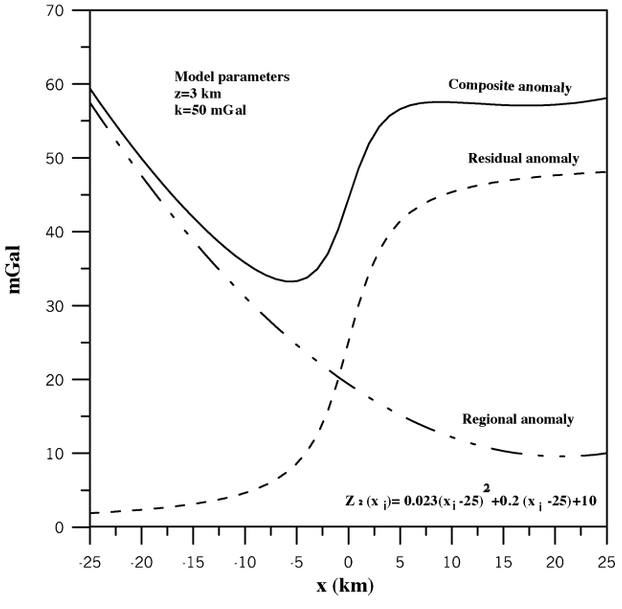

FIG. 6. Composite gravity anomaly Δg_3 of a buried faulted thin slab and a second-order regional.

In the case of the first composite gravity field, Table 2 shows that $z_1 = z_2 = z_3 = z_4$ and $k_1 = k_2 = k_3 = k_4$, which indicates that the correct order of regional is zero order, and z_1, and k_1 are the accurate depth and amplitude coefficients. On the other hand, in the case of the second composite gravity field, Table 2 shows that $z_1 \neq z_2 = z_3 = z_4$ and $k_1 \neq k_2 = k_3 = k_4$. This result indicates that the correct order of the regional of the second composite gravity field can be represented by a first-order polynomial, and z_2 and k_2 are the accurate model parameters. Finally, in the case of the third composite gravity field, it is verified numerically that $z_1 \neq z_2 \neq z_3 = z_4$ and $k_1 \neq k_2 \neq k_3 = k_4$ (Table 2), indicating the correct order of regional is second order, and z_3 and k_3 are the accurate depth and amplitude coefficient.

Random errors of 5% are added to each composite gravity field to produce noisy data. Three successive first-, second-, third-, and fourth-derivative graticule spacings ($s = 2, 3$, and 4 km) were applied to each composite input data. In this way, three sets of noisy first-, second-, third-, and fourth-derivative anomaly profiles are obtained from each composite gravity anomaly profile. Adapting the same interpretation technique described above, the results are shown also in Table 2 for the zero-, first-, and second-order noisy theoretical composite gravity fields.

Table 2 shows that average values of the depths and amplitude coefficients obtained from first-, second-, third-, and fourth-derivative anomalies computed from the first noisy composite gravity field are nearly equal (i.e., $z_1 \approx z_2 \approx z_3 \approx z_4$; $k_1 \approx k_2 \approx k_3 \approx k_4$. This result indicates that the optimum order of the regional gravity field is zero. On the other hand, in the case of the second theoretical composite gravity field, Table 2 shows also that $z_1 \neq z_2 \approx z_3 \approx z_4$; $k_1 \neq k_2 \approx k_3 \approx k_4$. As a result, the optimum order of the regional gravity profile is the first. Finally, in the case of the third composite gravity field, it is verified numerically (Table 2) that $z_1 \neq z_2 \neq z_3 \approx z_4$; $k_1 \neq k_2 \neq k_3 \approx k_4$. Accordingly, the optimum order of the regional gravity profile is the second . In all cases, the depth, the amplitude coefficient, and the optimum order regional gravity field are in good agreement with the actual ones, even when the data contain measurement errors. The results in Table 2 show that only a few points around the origin are sufficient to get the exact value of z and k. However, the data with random errors require more points around the origin (more graticule spacings are needed) to compute an accurate average depth and amplitude coefficient values from each derivative method.

APPLICATION TO FIELD EXAMPLE

To illustrate the practical application of the theory developed in the previous section, a field example from Egypt is

presented. Figure 7 shows the Bouguer anomaly profile over the Gazelle fault, south Aswan, Egypt. The fault affected both the basement and the sedimentary rocks, and crops out on the surface (Abdelrahman et al., 1999). This 5-km-long anomaly profile was digitized at interval of 0.125 km. The digitized values were subjected to separation techniques using the different derivative methods. In each derivative method, three successive graticule spacings were applied (Figures 8–11). Equations (6) and (8), (12) and (13), (15 and 16), and (18 and 19) were applied to determine the depth and amplitude coefficient of the fault $[(z_1, k_1), (z_2, k_2), (z_3, k_3)$, and $(z_4, k_4)]$ from the first-, second-, third-, and fourth-derivative anomaly values, respectively. The detailed results are shown in Table 3. Since the average values of the depth and amplitude coefficient obtained from the second-derivative anomaly values are nearly equal to those obtained from the third-derivative anomalies (Table 3), the regional gravity field can be represented by a first-order polynomial, and the depth and the amplitude coefficients of the fault given by the present method are 0.284 km and 11.6 mGal, respectively. Abdelrahman et al. (1991), using spectral analysis technique and gravity modeling, showed that the minimum depth to the basement complex in Aswan area is about 0.2 km and its maximum depth is 0.6 km. Thus the depth obtained by the present method is generally in good agreement with that obtained by Abdelrahman et al. (1991).

It is evident from this field example that the advantage of our method over continuous modeling methods (Abdelrahman et al., 1991) is that it requires neither density nor depth information, and it can be applied if little or no factual information other than the gravity data is available. It is also evident from the field example that our method gives good insight from gravity data of a long profile length concerning the nature of the fault structure. This is because the geological situation is not complicated. The present method may not be applied to real data in complex geologic situation to obtain reliable or detailed information about the different fault structures. This is true because each gravity measurement determines, at the station location, the sum of all effects from the surface downward. In complex geological situations, the gravity profile is seldom a simple picture of a single isolated disturbance but always is a combination of two or more anomalies of shallow origin and very broad anomalies of regional nature, which may have their origin below the section within which the geologic interest lies. The derivative analysis method can not be applied also in case of the presence of large-scale topographic features and near surface variations.

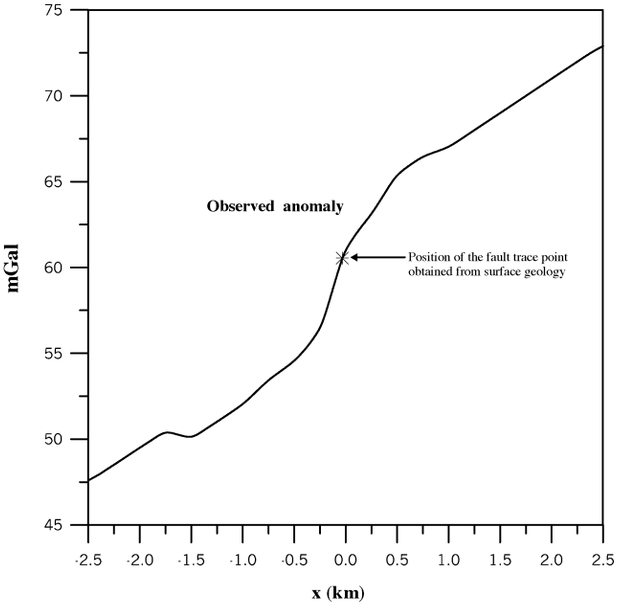

FIG. 7. Gazelle fault gravity anomaly, south Aswan, Egypt.

Table 2. Comparative study of depths and amplitude coefficients obtained from zero-, first-, and second-order synthetic examples.

Order of regional polynomial (p)	Graticule spacing (s) (km)	First-derivative method				Second-derivative method				Third-derivative method				Fourth-derivative method			
		Computed depth (z_1) from equation (6) (km)		Computed ampl. coeff. (k_1) from equation (8) (mGal)		Computed depth (z_2) from equation (12) (km)		Computed ampl. coeff. (k_2) from equation (13) (mGal)		Computed depth (z_3) from equation (15) (km)		Computed ampl. coeff. (k_3) from equation (16) (mGal)		Computed depth (z_4) from equation (18) (km)		Computed ampl. coeff. (k_4)from equation (19) (mGal)	
		Using data without random errors	Using data with random errors ±5%	Using data without random errors	Using data with random errors ±5%	Using data without random errors	Using data with random errors ±5%	Using data without random errors	Using data with random errors ±5%	Using data without random errors	Using data with random errors ±5%	Using data without random errors	Using data with random errors ±5%	Using data without random errors	Using data with random errors ±5%	Using data without random errors	Using data with random errors ±5%
Zero-order (p=0)	2	3	3.01	50	49.98	3	3.02	50	50.21	3	3.00	50	49.81	3	3.06	50	49.79
	3	3	2.99	50	49.93	3	3.03	50	50.17	3	3.03	50	50.39	3	3.00	50	50.40
	4	3	2.98	50	49.81	3	3.07	50	50.66	3	2.96	50	49.84	3	3.07	50	49.44
	Average values	3	2.99 ± 0.02	50	49.91 ± 01	3	3.03 ± 0.06	50	50.35 ± 0.27	3	3.00 ± 0.03	50	50.01 ± 0.32	3	3.05 ± 0.04	50	49.88 ± 0.49
First-order (p=1)	2	5.24	5.20	91.98	35.60	3	2.98	50	51.43	3	2.88	50	48.60	3	3.06	50	49.66
	3	5.77	5.62	96.26	34.33	3	3.31	50	50.63	3	3.07	50	49.56	3	3.06	50	49.88
	4	6.37	6.37	100.57	32.68	3	3.30	50	49.74	3	3.12	50	49.95	3	3.07	50	48.61
	Average values	5.79 ± 0.56	5.76 ± 0.59	96.63 ± 4.29	34.20 ± 1.46	3	3.20 ± 0.19	50	50.60 ± 0.85	3	3.02 ± 0.12	50	49.37 ± 0.69	3	3.06 ± 0.00	50	49.38 ± 0.68
Second-order (p=2)	2	1.41	1.39	25.62	25.23	3.21	3.03	53.62	49.46	3	2.88	50	48.60	3	3.06	50	49.66
	3	0.94	0.94	23.72	23.39	3.34	4.06	54.87	64.19	3	3.07	50	49.56	3	3.06	50	49.88
	4	0.68	0.73	22.97	22.78	3.53	4.27	56.24	65.28	3	3.12	50	49.95	3	3.07	50	48.61
	Average values	1.01 ± 0.37	1.02 ± 0.59	24.10 ± 1.36	23.80 ± 1.28	3.37 ± 0.16	3.78 ± 0.70	54.91 ± 1.35	59.64 ± 8.83	3	3.02 ± 0.12	50	49.37 ± 0.69	3	3.06 ± 0.01	50	49.38 ± 0.68

CONCLUSIONS

The problem of determining the depth and amplitude coefficient (related to the density contrast and the thickness) of a faulted thin slab from gravity data has been transformed into the problem of solving a nonlinear equation and a linear equation, respectively, using the least-squares method. Its also emphasized that numerical first-, second-, third-, and fourth-derivative gravity anomalies are useful tools for quantitative studies of gravity data. Determining the depth, amplitude coefficient of the buried fault, and the optimum regional gravity order is possible.

This method uses a faulted thin slab model convolved with the same first-, second-, third-, and fourth-derivative filter as applied to the observed gravity data. As a result, it can be applied not only to residuals but also to the Bouguer anomaly profile consisting of the combined effect of a residual component due to a purely local fault structure (shallow or deep) and a regional component represented by a polynomial of any order. The advantages of this technique over the correlation factors method are (1) the model parameters of the fault structures

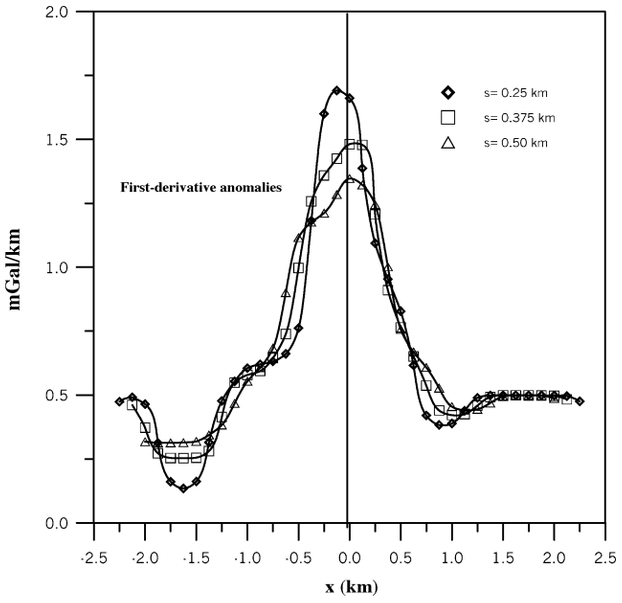

FIG. 8. Data analysis of Figure 7 using the first-derivative method.

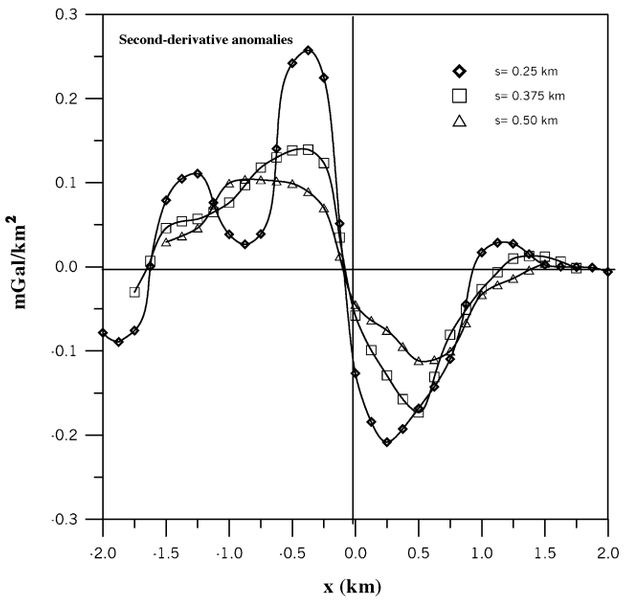

FIG. 9. Data analysis of Figure 7 using the second-derivative method.

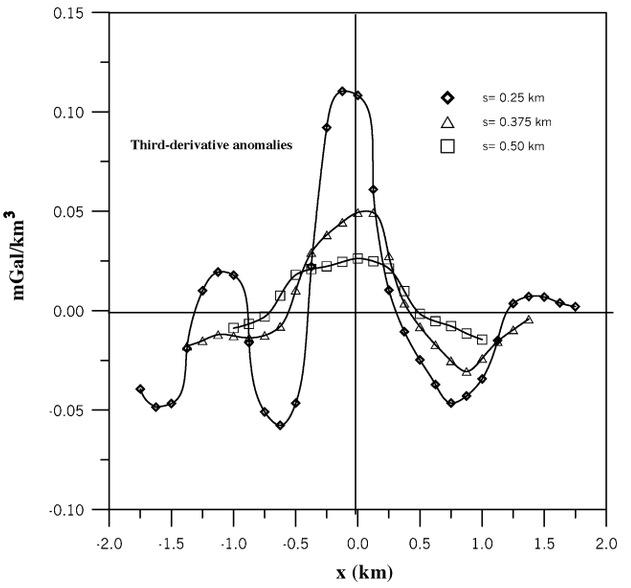

FIG. 10. Data analysis of Figure 7 using the third-derivative method.

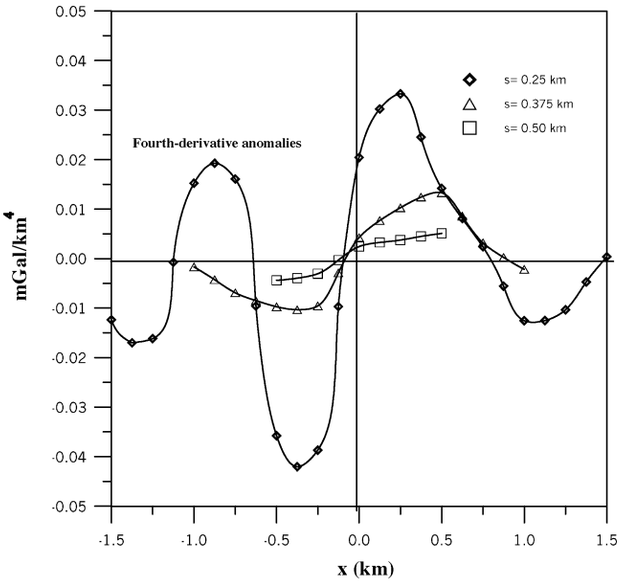

FIG. 11. Data analysis of Figure 7 using the fourth-derivative method.

Table 3. Numerical results of the field example.

Graticule spacing (km)	First-derivative method		Second-derivative method		Third-derivative method		Fourth-derivative method	
	Computed depth (z_1) from equation (6) (km)	Computed ampl. coeff. (k_1) from equation (8) (mGal)	Computed depth (z_2) from equation (12) (km)	Computed ampl. coeff. (k_2) from equation (13) (mGal)	Computed depth (z_3) from equation (15) (km)	Computed ampl. coeff. (k_3) from equation (16) (mGal)	Computed depth (z_4) from equation (18) (km)	Computed ampl. coeff. (k_4) from equation (19) (mGal)
0.250	0.591	24.40	0.305	12.22	0.306	12.70	0.299	12.40
0.375	0.666	25.73	0.271	11.16	0.314	12.58	0.304	12.20
0.500	0.724	26.66	0.277	11.41	0.312	12.46	0.674	14.38
Average values	0.660 ± 0.07	25.6 ± 1.14	0.284 ± 0.02	11.60 ± 0.56	0.311 ± 0.01	12.58 ± 0.12	0.426 ± 2.2	12.99 ± 1.21

can be determined automatically, and (2) it can be applied to interpret all gravity data points acquired over a large area of the buried structure (i.e., from the large segment of the gravity anomaly profile around the origin). The disadvantage of the present least-squares derivative analysis method of interpretation relative to standard methods is that it cannot be applied in complex geologic situations or areas with large-scale topographic and near-surface density variations.

ACKNOWLEDGMENTS

The authors thank the editors and the two capable reviewers for their excellent suggestions. Many thanks to Dr. John W. Peirce, the associate editor, for his keen interest, valuable comments on the manuscript, and improvements to this work. Thanks are also due to Judy Wall and Sheral Danker at SEG, and Dr. M. H. Kamel and Mr. K. S Essa, Geophysics Department, Faculty of Science, Cairo University, for their assistance.

REFERENCES

Abdelrahman, E. M., Bayoumi, A. I., Abdelhady, Y. E., Gobashy, M. M., and El- Araby, H. M., 1989, Gravity interpretation using correlation factors between successive least-squares residual anomalies: Geophysics, **54**, 1614–1621.

Abdelrahman, E. M., Radwan, A. H., Issawy, E. A., El-Araby, H. M., El-Araby, T. M., and Abo-Ezz, E. R., 1999, Gravity interpretation of vertical faults using correlation factors between successive least-squares residual anomalies: The Mining Přibram Symp., Mathematical Methods in Geology, MC2-1-6.

Abdelrahman, E. M., Riad, S., Refai, E., and Amin, Y., 1985, On the least-squares residual anomaly determination: Geophysics, **50**, 473–480.

Abdelrahman, E. M., Tealeb, A. A., and Ahmed, H. A., 1991, Gravity map of Kalabsha area, northwest of Aswan Lake, and its structural significance: Geodynamics, **14**, 125–135

Agarwal, B. N. P., and Lal, T., 1971, Application of rational approximation in calculation of the second derivative of the gravity field: Geophysics, **36**, 571–581.

Bhattacharyya, B. K., 1976, Recursion filters for digital processing of potential field data: Geophysics, **41**, 712–726.

Geldart, L. P., Gill, D. E., and Sharma B., 1966, Gravity anomalies of two-dimensional faults: Geophysics, **31**, 372–397.

Grant, F. S., and West, G. F., 1970, Interpretation theory in applied geophysics: McGraw-Hill Book Co.

Griffin, W. R., 1949, Residual gravity in theory and practice: Geophysics, **14**, 39–58.

Gupta, O. P., 1983, A least squares approach to depth determination from gravity data: Geophysics, **48**, 375–360.

Hedstrom, H., 1938, A new gravimeter for ore prospecting: Am. Inst. Min. Met. Eng. Tech. Pub. **953**, 1–23.

Hubbert, M. K., 1948, Gravitational terrain effects of two-dimensional features: Geophysics, **13**, 226–254.

Lines, L. R., and Treitel, S., 1984, A review of least-squares inversion and its application to geophysical problems: Geophys. Prosp., **32**, 159–186.

Mesko, A., 1984, Digital filtering application in geophysical exploration for oil: Akademiai Kiado, Pitman Publishing Ltd., and Halstedpress.

Nettleton, L. L., 1976, Gravity and magnetics in oil prospecting: Mc-Graw Hill Book Co.

Press, W. H., Flannery, B. P., Teukolsky, S. A., and Vetterling, W. T., 1986, Numerical recipes: The art of scientific computing: Cambridge Univ. Press.

Xia, J., Sprowl, D. R., and Steeples, D. W., 1996, A model of Precambrian geology of Kansas derived from gravity and magnetic data: Computers & Geosciences, **22**, 883–895.

Zeng, H., 1989, Estimation of the degree of polynomial fitted to gravity anomalies and its applications: Geophys. Prosp., **37**, 959–973.